

Topological correlations in Bénard-Marangoni convective structures

P. Cerisier,¹ S. Rahal,¹ and N. Rivier²

¹*Institut Universitaire des Systemes Thermiques Industriels, UMR CNRS 139, Université de Provence, 13397 Marseille Cedex 20, France*

²*Laboratoire de Physique Théorique, Université Louis Pasteur, 3 rue de l'Université, 60874 Strasbourg, France*

(Received 6 November 1995; revised manuscript received 13 May 1996)

Bénard-Marangoni convection displays a two-dimensional (2D) hexagonal pattern. A topological analysis of these structures is presented. We describe the elementary topological transformations involved in such patterns (neighbor switching process, cell disappearance or creation, and cellular division) and the typical defects [pentagon-heptagon pair, “flower” (a cluster of more than three polygons incident on the same vertex), etc.]. Usual topological laws (Lewis’s, Aboav-Weaire’s, Peshkin’s, and Lemaître’s laws) are satisfied. For Von Neumann’s law, a modification which takes into account a physical effect specific to the dynamics of Bénard-Marangoni structures (selection of average cell size in steady regime) has been introduced. We also compare topological correlations in Bénard-Marangoni structures with those derived from biological tissues or simulated structures (2D hard disk tessellations, Ising mosaics, distributions of maximum entropy formalism, etc.). The agreement is fair for pentagons, hexagons, and heptagons. [S1063-651X(96)06811-0]

PACS number(s): 47.20.Dr, 02.50.-r, 64.60.Cn, 05.40.+j

I. INTRODUCTION

As emphasized by various authors [1–3] random cellular structures, froths (in three dimensions), and mosaics (in two dimensions) abound in nature and are of interest in many scientific fields such as metallurgy [4,5], geology [6], biology [7,8], or ecology [9,10]. In spite of the variety of constituent materials and forces responsible for their architecture, these structures look geometrically identical. In practice, we have to distinguish between evolutive mosaics, where the number of cells (and sometimes the total area) changes with time, such as biological tissues [8], polycrystallization processes [11], and nonevolutive mosaics where the number of cells (and total area) remains constant, as in metallurgical cuts or tessellations built from point or disk packings [12–14].

Here, we investigate the cellular structure generated by Bénard-Marangoni convection (also called surface-tension-driven Bénard convection). A fluid heated from below and with a free upper surface exhibits convection motion beyond a certain value of the vertical gradient temperature (ΔT_c : critical value) and one observes a two-dimensional (2D) cellular pattern on the free surface (Fig. 1). The convective phenomenon is three dimensional but an evolutive two-dimensional mosaic of convective cells is observed over a constant area.

This cellular structure is deformable but, as in crystals, it contains dislocations and grain boundaries. This similarity with crystal systems leads, using techniques and tools of crystallography, to a description of the dynamics and to an estimate of the amount of disorder in Bénard-Marangoni patterns [15–19]. It seems that no topological analysis has been devoted until today to Bénard-Marangoni structures. So, the aims of this work are, first, to describe the dynamics of Bénard-Marangoni structures through elementary topological transformations, to describe the typical defects observed, to carry out the topological analysis of these patterns through correlation and metric laws, and, finally, to compare its correlation values with those of other natural or simulated struc-

tures with similar statistical characteristic [such as variance μ_2 of the distribution $P(n)$ defined below].

Topological characterization of such structures always includes the distribution $P(n)$ of the number n of sides of cells (here, called n -cells), the variance μ_2 of the distribution $P(n)$, the mean number $m(n)$ of sides of the first-neighbor cells of n -cells, the average area $\langle A_n \rangle$ of n -cells, and the topological correlation function $A_{kn} = M_k(n)/P(k)$, where $M_k(n)$ is the average number of k -sided neighbors of n -cells, [clearly, $nm(n) = \sum_k k M_k(n)$].

The outline of this paper is the following. The experimental procedure is described in Sec. II. Our results are given in Sec. III and they are compared, when possible, to other natural, simulated structures or distributions derived from theoretical models with similar statistical characteristic. Finally, some conclusions are given in Sec. IV.

II. EXPERIMENTAL PROCEDURE

The experimental setup consists of a thin (4.3 mm) horizontal layer of silicon oil Rhodorsil 47V100 (Prandtl num-

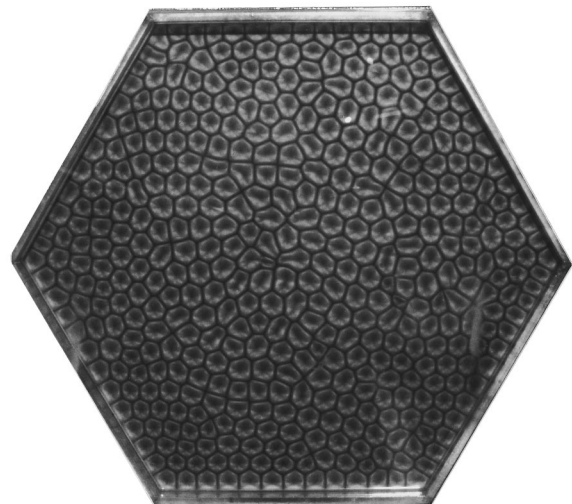


FIG. 1. Cellular structure in Bénard-Marangoni convection.

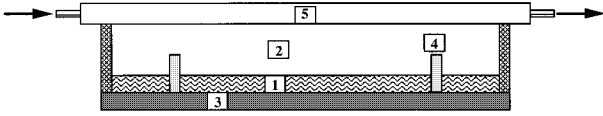


FIG. 2. Schematic description of the apparatus 1: Fluid layer; 2: Air; 3: Container; 4: Vessel; 5: Cooling container.

ber $Pr=880$ at $25\text{ }^\circ\text{C}$) set in a container with a flat copper bottom (in which an electric resistance is embedded to provide a uniform temperature) and lateral walls made of Plexiglass. The vessel limiting the part of the layer under investigation is surrounded by an outer guard ring of the same oil. This ring, and the fact that Plexiglass has about the same thermal conductivity as the silicon oil guarantee a quasiadiabaticity of the sidewalls. The fluid was cooled from above through a thin layer of air. The air was bounded on top by a glass plate, which is itself the bottom of a container in which water, coming from a bath with regulated temperature, circulates in order to fix the temperature of the glass plate and thereby the temperature on top of the fluid. The essential features of the apparatus described above are shown in Fig. 2. The temperatures at the upper and lower surfaces are measured by means of thermocouples, the precision of the measurements is about $0.1\text{ }^\circ\text{C}$. The liquid depth (d), is measured by means of a micrometer with a precision of 0.01 mm . Flow visualization was achieved by aluminum powder suspended in the fluid or by a shadowgraph technique. Photographs of the convective structure are taken at regular time intervals for a long period (up to 10 days). Then the photographs are digitized. Appropriate filterings and scalings provide a binary image. Suitable software allows us to obtain the values of the relevant functions. The surface temperature field is obtained by infrared thermography [20].

The confinement of the fluid layer is taken into account by means of a nondimensional parameter, the aspect ratio Γ , which is the ratio of a characteristic horizontal length to the liquid depth, $\Gamma = \sqrt{S}/d$ (S is the surface area of the pattern). A hexagonal vessel is used, because it has been observed [21] that this geometrical form induces a minimal disorder. Experiments have been performed in a vessel with $\Gamma=65$, this value corresponds to medium confinement. Under these conditions, wall effects exist but the hexagonal shape does not induce any extrinsic disorder and it allows for plasticity of the structure and for the existence of a certain amount of intrinsic disorder.

The external parameter which controls the instability is the temperature difference ΔT across the layer. Usually, it is more useful to take a normalized parameter, the distance to the threshold

$$\epsilon = \frac{R - R_c}{R_c} = \frac{M - M_c}{M_c}. \quad (1)$$

where R and M are, respectively, the Rayleigh and Marangoni numbers, and the subscript (c) stands for the corresponding threshold value. Experiments are performed at $\epsilon=2.5$.

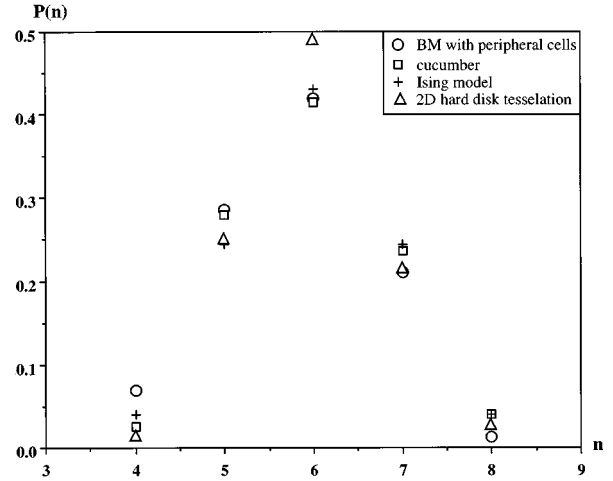


FIG. 3. Distribution $P(n)$ of the number n of sides of cells for natural and simulated structures for $\mu_2=0.812$.

III. RESULTS AND DISCUSSION

The discussion of random area-filling cellular patterns (mosaics) is based on a few simple topological considerations. The mosaics consist of cells, bounded by edges, incident on vertices with valence Z . The only topological random variable is n , the number of sides of a cell. If the mosaic is random and in the absence of adjustment, there are always $Z=3$ edges and cells incident on a vertex. It follows that $\langle n \rangle = 6$; cells are six sided on average in a large mosaic. For an example of random structures with adjustment, see the work of Simon and Belmedani [22] who observed, in thermosolutal structures of horizontal layers of aqueous solutions of sucrose evaporating freely, many vertices with $Z>3$ and $\langle n \rangle < 6$. For Bénard-Marangoni structures, when peripheral cells (cells in contact with sidewalls) are not taken into account, $\langle n \rangle = 6$. Since peripheral cells are overwhelmingly pentagonal, $\langle n \rangle$ is between 5 and 6 when they are taken into account.

There are several models for random mosaics: Voronoi tessellations [23] (used also in the construction of structures in “2D hard disk” tessellation [24], in air table packings [25,26], and in colloidal aggregation [27]), maximum entropy mosaics [28–30] and Ising-model construction [31,32] are all well reviewed in the literature. Here we will compare our data with those of the above structures.

The Bénard-Marangoni structures exhibit a distribution of the number of cell sides mainly with $4 \leq n \leq 8$, such as various natural (biological tissues [8], cellular arrays obtained in directional solidification of alloys [33]), or simulated structures [24,34]. All these structures have $\mu_2 \leq 1.7$.

In order to compare the Bénard-Marangoni structures with their natural counterparts (the so called 220 mm cucumber tissue [7]), and with the structures obtained by the Ising model [31,32], and simulated “2D hard disk” tessellations [34], we selected structures with the same variance $\mu_2 (=0.812)$ of the $P(n)$ distribution. Figure 3 shows the topological distribution $P(n)$ as a function of n for $\mu_2=0.812$ for the structures mentioned above. It can be seen that the $P(n)$ distribution observed in these natural or simulated cellular arrays agree satisfactorily with the distribution obtained in Bénard-Marangoni mosaics. The asymmetry of

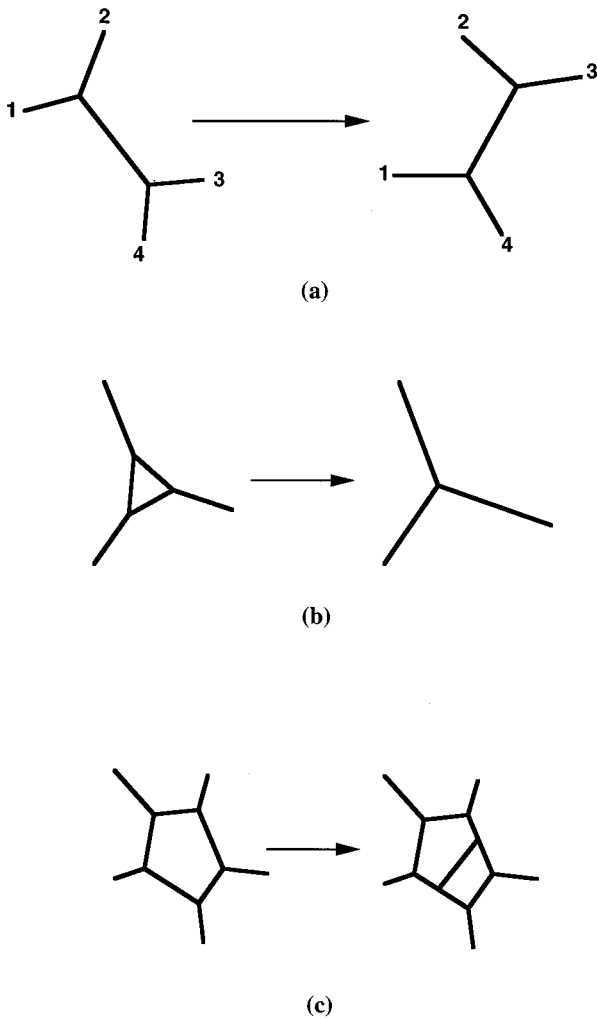


FIG. 4. Elementary topological transformation: (a) neighbor switching (T_1 process); (b) cell disappearance (T_2 process); (c) cell division.

the Bénard-Marangoni distribution is due to the fact that (mostly pentagonal) peripheral cells have been taken into account.

A. Elementary topological transformations and different typical defects

The two types of elementary topological transformations (ETT) by which a perfect hexagonal pattern might be progressively modified to produce a disordered structure, or by which a structure evolves in time, are well known [3,35]. First, there is the neighbor switching process (T_1 process) [Fig. 4(a)]; second, cell disappearance or creation (T_2 process) [Fig. 4(b)], and cellular division [Fig. 4(c)] which is a composition of T_1 and T_2 [35].

Neighbor switching (T_1) is a fast transformation, whose effects are rapidly relaxed. Accordingly, it is extremely rare in soap froths. In mosaics with a fixed number of cells, such as Voronoi mosaics, T_1 is the only topological transformation and it is solely responsible for statistical equilibrium. On the other hand, T_2 is a slow transformation, and it constitutes the main agent of slow coarsening of the soap froth or of

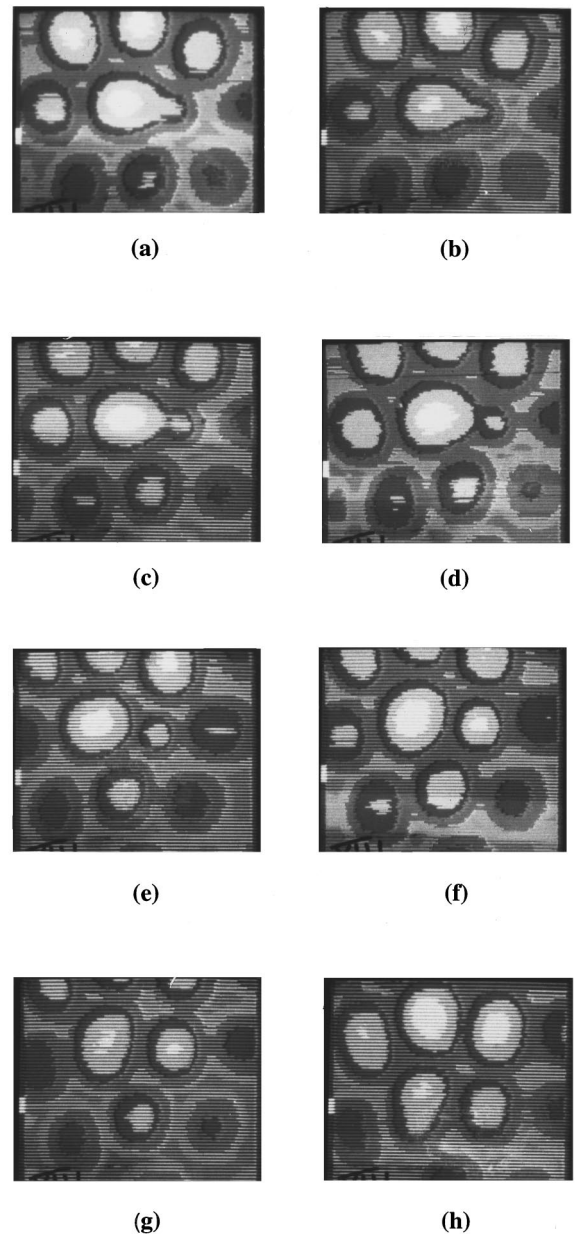


FIG. 5. Creation of a new cell in Bénard-Marangoni structures, observed by infrared thermography.

polycrystals in metallurgy, where coalescence of subgrains is observed. Cell division (mitosis) is responsible for the steady state of biological tissues, and for their efficient, local response to an injury [35].

In the dynamics of Bénard-Marangoni structures in small vessels, a T_1 process has been observed by Ondaçuhu *et al.* [36]. We have often observed coalescence of two adjacent cells into one, or the progressive disappearance of a cell which is getting smaller and smaller. We have also observed the “birth” of a new cell which occurs by scission of the “mother” cell. This is shown in Fig. 5 which exhibits the evolution of the surface temperature field. At first (a), the liquid is moving upward on the central axis of a 7-cell. Then the 7-cell becomes elongated and at the same time the liquid moves upward along a vertical central planar region [this plane is directed from left to right in Figs. 5(b) and (c)]. A “daughter cell” appears (d). Then the size of the daughter

cell increases (d)–(g). This phenomenon is observed to take about 1 h. The process is reversible: disappearance of a cell by the inverse process is often observed. Moreover, the process can stop at stages (d) or (e) and return to (a): this reversal occurs when a faster “birth” takes place in the neighborhood. This division process is very similar to mitosis in biological tissues, the region of upward moving liquid playing the part of the nucleus of the cell [35]. So, in Bénard-Marangoni structures, we have observed all the ETT, which makes it a more complex and more interesting cellular structure to study.

In Bénard-Marangoni structures, polygons with 4 to 8 sides are observed. The 4-cells and 8-cells are absent or very few and they have a very short lifetime. All cells, except those with six sides, are considered as defects. As in crystallography, one characterizes these defects by surrounding them with a contour. The contour closes if it does not surround any defect. The Burgers vector of a defect measures this lack of a closure. In Bénard-Marangoni structures, the most common defects are the pentagon-heptagon pair and the “flower” defect. The pentagon-heptagon pair is a dislocation in a hexagonal lattice, with Burgers vector 1 [Fig. 6(a)]. The “flower” defect, which is a cluster of more than three polygons, incident on the same vertex, has zero total Burgers vector and the same contour as a cluster of several (regular or irregular) 6-cell. Figures 6(b), 6(c), and 6(d) exhibit the three possible varieties. This defect is not topologically stable; it disappears (slowly) by T_1 transformation and the regular lattice is restored.

Pairs of dislocations [i.e., two dipoles (5-cell+7-cell)] are also observed. Two typical arrangements are shown in Figs. 6(e) and 6(f). The pairs share a common edge between a pentagon and a heptagon [Fig. 6(e)] or are separated by a hexagon [Fig. 6(f)]. In both cases, the total Burgers vector is 2, but the two dislocations are oriented differently. We have also observed cases where the dislocations share a common edge of their pentagons. The two dislocations have then opposite Burgers vectors and the total Burgers vector is zero. Lewis [37] and Pyshnov [38] have noticed that this is the topological defect created by mitosis in biological tissues. Pairs of dislocations, also with zero total Burgers vector but with a common edge between heptagons, can be created under shear. This process has not been observed in our Bénard-Marangoni structures.

We have observed also two “flowers” in contact [Fig. 6(g)], with the two “flowers” composed of five and six cells, respectively. The resulting Burgers vector is 1. Finally, aggregates of a “flower” defect and a dislocation have been seen, [Fig. 6(h)], with a Burgers vector of 2.

B. Topological laws

1. Lemaître’s law

A global measure of the “disorder” of a pattern may be given by the variance μ_2 of the topological distribution $P(n)$ which measures the deviation of the structure with respect to the perfect hexagonal pattern:

$$\mu_2 = \langle n^2 \rangle - \langle n \rangle^2. \quad (2)$$

Soap froths have $1 \leq \mu_2 \leq 3$. Biological tissues have μ_2 of the order of unity. In the mosaics generated numerically by

Peshkin, Strandburg, and Rivier [34] $\mu_2=8-12$. For the discs on an air table [25] $\mu_2 \leq 1.75$. The value $\mu_2=1.75$ seems to be the limiting value for two-dimensional points systems [12,13]. For Bénard-Marangoni structures, we have found $0.2 \leq \mu_2 \leq 0.8$.

It is therefore interesting to plot (Fig. 7) the variance μ_2 against $P(6)$, for different mosaics. All data fall on the same curve with very good accuracy in spite of the variety of their origins. We confirm the results of Lemaître *et al.* [26] who were the first to suggest that the equation of state $\mu_2=f(P(6))$ could be universal in mosaics. The fact that this universality is a consequence of maximum entropy formalism (MEF) was demonstrated later [39]. Figure 7 shows that peripheral cells increase μ_2 and the dispersion of the Bénard-Marangoni data points. Indeed, most peripheral cells are pentagons which decrease $P(6)$ and increase μ_2 . Generally, Bénard-Marangoni structures without peripheral cells have only hexagonal, pentagonal, and heptagonal cells. In this case, $\mu_2=1-P(6)$, regardless of the distribution, and this asymptotic behavior is manifest in Fig. 7, for $P(6)>0.6$.

Figure 8 shows that data points from Bénard-Marangoni structures lie only on the theoretical curve [39] with good accuracy. It also shows that our data superpose well on those of various authors. Experimentally, we find that data points lie on a plateau corresponding to $\mu_2 P(6)^2 = 0.16 \pm 0.01$ for $P(6) < 0.7$ as predicted by various authors [39,40]. Figures 7 and 8 support the suggestion of Lemaître *et al.* [26] and the maximum entropy inference [39] that all froths follow the same structural equation of state (Lemaître’s law).

2. Aboav-Weaire’s law

ETT are local transformations, which, like the collisions in gases, keep the cellular structure in statistical equilibrium. The observable manifestation of this fact is given by the Aboav-Weaire relation [3,11]. It states that the mean number $m(n)$ of sides of the first-neighbor cells of n -cells $m(n)$ is related to n by

$$m(n) = 6 - a + \frac{(6a + \mu_2)}{n}, \quad (3)$$

where μ_2 is the variance of the $P(n)$ distribution. We shall comment on the value of a below.

We have plotted the product nm versus n at different times in the Bénard-Marangoni experiment. In all cases, $nm(n)$ is linear in n , but with a different slope ($6-a$) from the value suggested in [11]. The parameter a should be one in all evolutive mosaics (mosaics with cell division or disappearance). This is the case of biological cells [8], polycrystals [11], and nearly verified for soap froths [11] and diffusion-limited cluster aggregation (DLCA) [27]. The Monte Carlo-generated mosaics of Peshkin, Strandburg, and Rivier [34] are dominated by neighbor exchanges, cell disappearance is only a small perturbation. Consequently, a is large and negative. Random Voronoi polygons generated from two-dimensional Poisson point process are nonevolutive and have $a=0.5$ [41].

Figure 9 shows that, in Bénard-Marangoni structures, a increases slowly with time from $a=1.06$ to $a=2.08$ and then decreases towards an asymptotic value (≈ 1.4). This behavior is due to the dynamic of the Bénard-Marangoni structures.

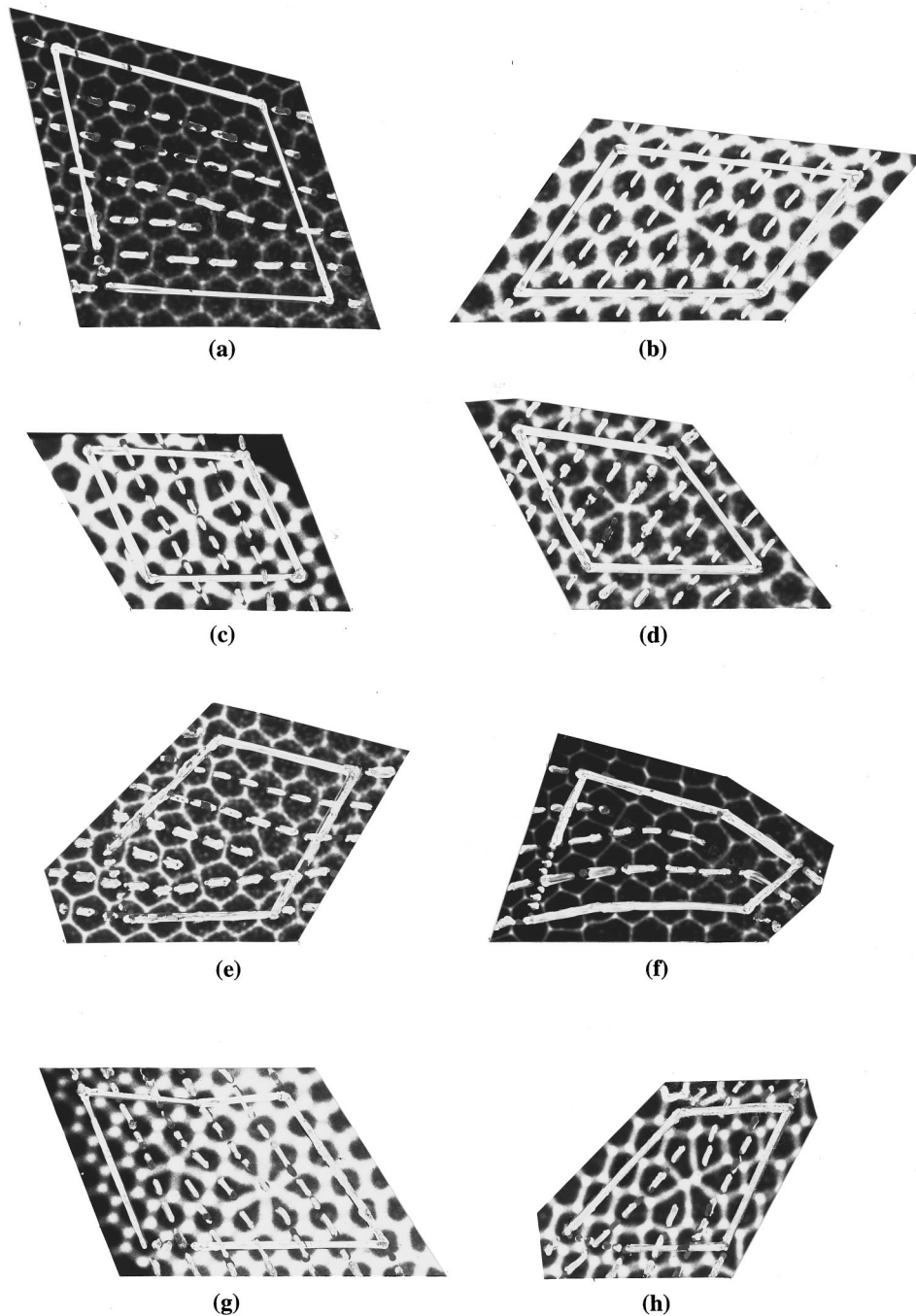


FIG. 6. Typical defects in Bénard-Marangoni structures and their arrangement. (a) Basic defect (5-cell+7-cell). The corresponding dislocation has Burgers vector 1; (b), (c), and (d) “flower” defects with Burgers vector zero; (e) and (f) pair of dislocation (5-cell+7-cell). The total dislocation has Burgers vector 2; (g) Two “flower” defects in contact with a Burgers vector of 1; (h) arrangement of a “flower” defect and a dislocation.

First, the increase of a corresponds to the evolution of the structure in the transient regime, then the abrupt decrease of a for $t \approx 125$ h corresponds to the fast relaxation of the structure towards the steady regime characterized by fluctuations around a mean value. The same trend (increase followed by decrease of a) was observed with $0.7 \leq a \leq 1.4$ in the air table experiments of Lemaître *et al.* [25] but as a function of the concentration, instead of the time in our case. In reaction-limited cluster aggregation (RLCA), a also changes with time [27].

Note that $m(6)$ is independent of a

$$m(6) = 6 + \frac{\mu_2}{6}. \quad (4)$$

This relation is verified by our experiments, which are fitted by

$$m(6) = 5.95 + 0.17\mu_2. \quad (5)$$

Likewise, the Weaire identity [2]

$$\langle nm(n) \rangle = \mu_2 + \langle n \rangle^2, \quad (6)$$

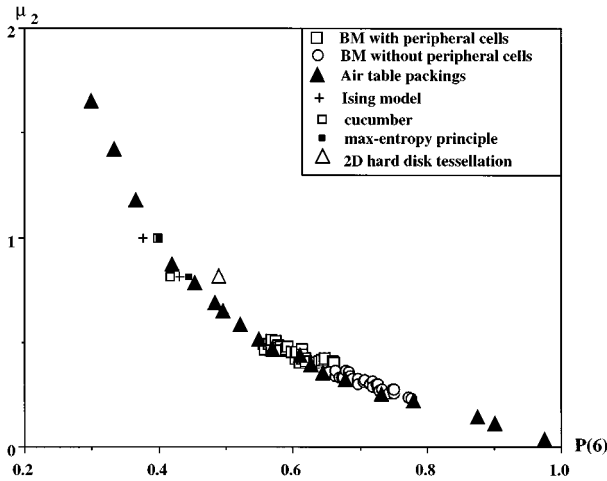


FIG. 7. Variance μ_2 against $P(6)$ for several natural or simulated structures.

holds in Bénard-Marangoni structures.

3. Metric law: Lewis's law

Lewis's law [7] was discovered in cucumber epidermis, human amnion (*sic*), and pigmented epithelium of the retina. It holds in many other epithelial tissues [8]. Later, Rivier and Lissowski [42] demonstrated that Lewis's law actually is a mathematical law which has to be satisfied by any random space-filling structure maximizing its entropy.

Lewis's law states that the average area of n -sided cell $\langle A_n \rangle$ increases linearly in n

$$\langle A_n \rangle = S(n - n_0). \quad (7)$$

Soap froths obey Lewis's law [notwithstanding the few, not statistically significant 3- and 4-sided cells, which would have a negative $\langle A_3 \rangle$ or $\langle A_4 \rangle$ from Eq. (7)]. It is obeyed in air table packings [25] (but only for low concentrations of disks; steric effects spoil the linearity at higher concentrations [43])

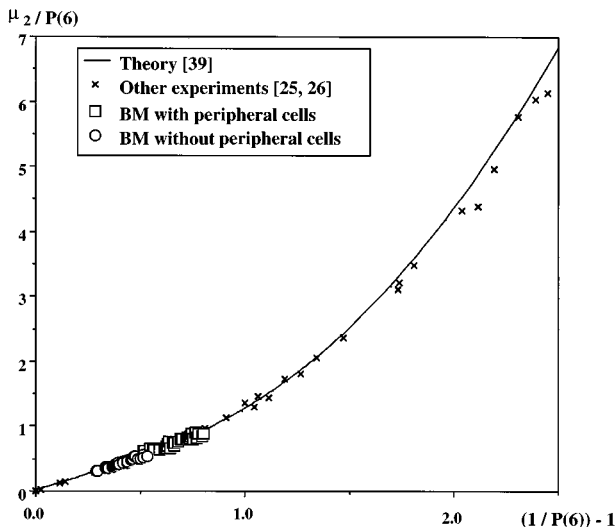


FIG. 8. Virial equation of state: $\mu_2/P(6)$ as function of $1/P(6) - 1$. Bénard-Marangoni points, and other experimental data points superposed to the theoretical curve [39].

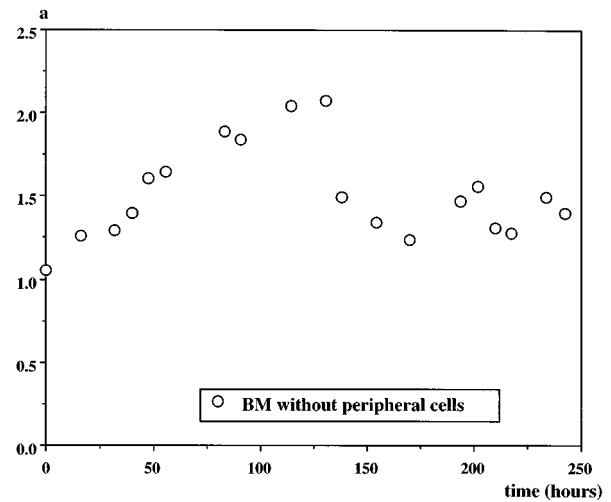


FIG. 9. Parameter a of the Aboav-Weaire's law as function of the real time in Bénard-Marangoni experiment.

and in diffusion-limited cluster-cluster aggregation DLCA [27]. Cellular arrays formed during directional solidification of a binary Pb-Tl alloy [33] obey this law with $n_0=2$. In thermosoluted structures of layers of aqueous solution of sucrose [22], Lewis's law is also satisfied with $n_0=2.47$. We verified that in the Bénard-Marangoni experiments $\langle A_n \rangle$ is linear in n at all times, the Lewis's law is satisfied.

Furthermore, it has been shown [44] that the slope S and intercept n_0 of the Lewis line are linked to a parameter λ , which, in a coarsening structure, measures its aging by the relations

$$S = \lambda \langle A \rangle, \quad (8)$$

$$n_0 - 6 + \frac{1}{\lambda} = 0. \quad (9)$$

In soap froths, λ is increasing linearly with time, a consequence of Von Neumann's law [45]. Thus, the larger λ , the larger the slope S and the intercept n_0 , the coarser and older is the structure. By contrast, biological tissues do not coarsen, but evolve in a steady state, and only the slope of Lewis's law may increase with time as the tissue ages (through $\langle A \rangle$), while the intercept n_0 (and λ) remains constant. In our case, both the intercept n_0 and the slope S change with time. These variations, as functions of time, have an effect on λ . Figure 10 shows the variation of λ , obtained from the intercept (Eq. 9), in real time for Bénard-Marangoni structures. It can be seen that, first, λ increases and then reaches a plateau at about $\lambda=0.23$. It can be noticed that the steady regime, corresponding to this plateau, is reached for the same time ($t \approx 125$ h) as for the parameter a of the Aboav-Weaire law. This behavior can be explained as follows: Lewis's law can be differentiated in time, to yield [44] a version of Von Neumann's law (averaged over n -sided cells),

$$\frac{d\langle A_n \rangle}{dt} = \left[\frac{d}{dt} \langle A \rangle \lambda \right] (n - 6) + \frac{d}{dt} \langle A \rangle, \quad (10)$$

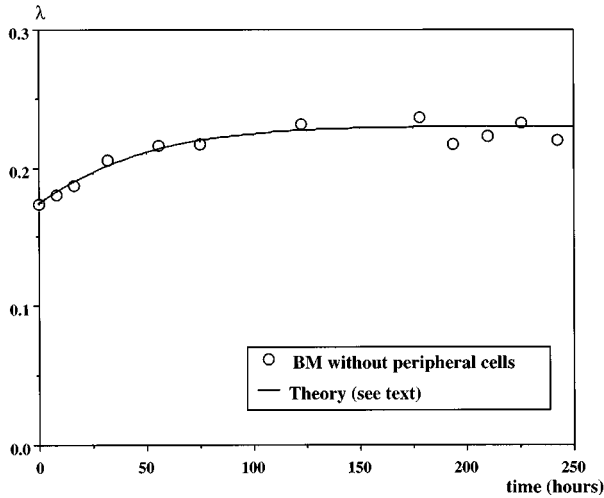


FIG. 10. Lewis's law: Parameter λ as function of the real time in the Bénard-Marangoni experiment.

where $\langle A \rangle(t)$ is the averaged cell area at time t . A Bénard-Marangoni structure evolves towards a steady regime and selects its mean wavelength or its average cell size A_{sel} . Thus

$$\frac{d\langle A \rangle}{dt} = -\alpha(\langle A \rangle - A_{\text{sel}}), \quad (11)$$

has a solution

$$\langle A \rangle(t) = A_{\text{sel}} + (A_0 - A_{\text{sel}})\exp(-\alpha t), \quad (12)$$

in terms of the initial cell size $A_0 = \langle A \rangle(t=0)$.

There is no diffusion of matter driving the evolution of the structure (the energy is not concentrated at the interface), so that the evolution equation (10) for a n -sided cell in a Bénard-Marangoni structure should be independent of n , thus $d(\langle A \rangle \lambda)/dt = 0$. Using the known evolution of $\langle A \rangle$ with time [Eqs. (11),(12)], we obtain

$$\frac{1}{\lambda} \frac{d\lambda}{dt} = \frac{\alpha}{[1 + \mu \exp(\alpha t)]}, \quad (13)$$

where $\mu = A_{\text{sel}}/(A_0 - A_{\text{sel}})$. The solution is

$$\lambda(t) = \lambda_0 \frac{\mu + 1}{\mu + \exp(-\alpha t)}. \quad (14)$$

$\lambda(t)$ is plotted in Fig. 10. The best fit with experiment gives $\alpha = 0.25$, with $\lambda_0 = \lambda(t=0)$. If $[d(\langle A \rangle \lambda)/dt]$ had been different from zero, the coefficient λ would keep on increasing in time, which is not the observed behavior.

4. Correlation functions: Peshkin's laws

Peshkin *et al.* [34] have drawn attention to a nearest-neighbor correlation $M_k(n)$ which is the average number of k -sided neighbors of an n -cell and to a topological correlation function $A_{kn} = M_k(n)/P(k)$. $M_k(n)$ satisfies two identities, a sum rule

$$\sum_k M_k(n) = n, \quad (15)$$

which states that cells with n sides have n neighbors, and a symmetry relation for the number of edges between n and k -sided cells

$$M_k(n)P(n) = M_n(k)P(k); \quad (16)$$

thus, $A_{kn} = A_{nk}$ with an obvious inequality

$$A_{kn} \geq 0 \quad \text{for all } n, k. \quad (17)$$

Maximum entropy formalism [32,34,40] yields a linear dependence of A_{kn} with n (or k)

$$A_{kn} = (n-6)\sigma(k-6) + n + k - 6, \quad (18)$$

where $\sigma = -(a/\mu_2) \leq (1/6)$ is a structural parameter. A froth without correlation has $\sigma = (1/6)$. For most natural structures, ($a=1$), $\sigma = -(1/\mu_2)$.

Figure 11 shows the five A_{kn} ($k=4-8$) as functions of n for the various natural or simulated structures (the 220 mm cucumber tissue [7], structures obtained from Ising model [31,32], maximum entropy mosaics [34] and simulated "2D hard disk" tessellation [24]) all at the same value of the variance $\mu_2 = 0.812$. Straight lines are given by Eq. (18). Assuming that simulated structures also have $a \approx 1$, there should be agreement between the A_{kn} of the Bénard-Marangoni structures and those derived from the other structures. The agreement is reasonable for $n=5-7$. The maximum difference between Bénard-Marangoni data and maximum entropy predictions is at most 10%.

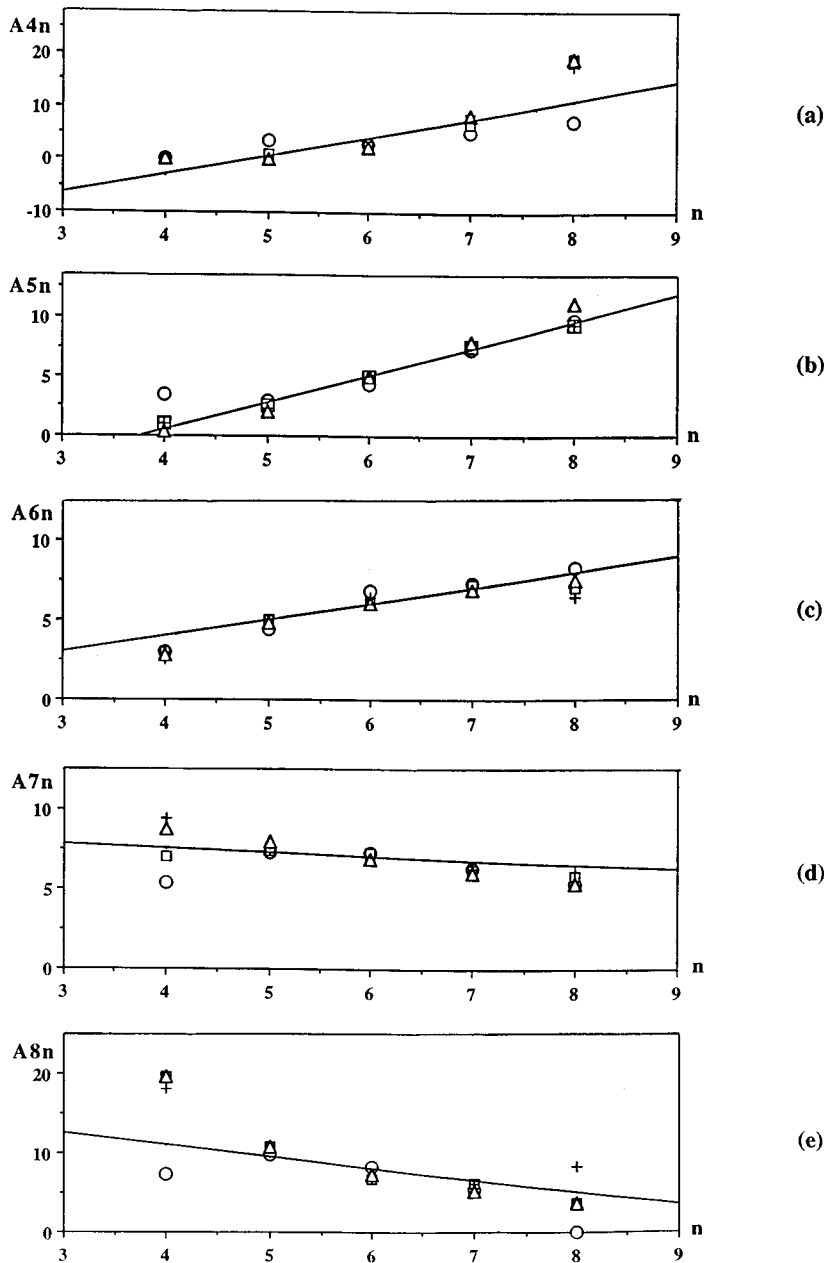
Whereas the maximum entropy prediction for A_{kn} is linear in n , some random numerical tessellations (Ising model [32] and hard disk tessellations [24]) give a dependence in n which is more quadratic than linear. Given that there are very few 4- and 8-cells, the topological correlation functions between 4- or 8-cells and with 5-, 6-, or 7-cells are not statistically significant. Taking into consideration only the A_{kn} ($k=5-7$, $n=5-7$) we can conclude that the Bénard-Marangoni structures follow fairly well the theoretical expression (18).

IV. CONCLUSIONS

This paper has analyzed Bénard-Marangoni structures in topological terms. We emphasize that we have been dealing here only with Bénard-Marangoni structures (free upper surface), which are cellular and random [18-21,35,46,47], whereas Rayleigh-Bénard structures (fixed upper surface) are chiefly ordered rolls. They have been discussed extensively in the literature [47,48].

We carried out a study of the slow dynamics of these structures and we compared them to other natural structures, or to structures built from models involving elementary topological transformations. This study confirms the applicability to Bénard-Marangoni structures of general topological laws such as Aboav-Weaire's, Lewis's, Lemaître's, and Peshkin's laws.

All the ETT which have been otherwise observed in one structure or another are involved together in the dynamics of



(a)

(b)

(c)

(d)

(e)

FIG. 11. Topological correlation functions A_{kn} as function of n for natural and simulated structures for $\mu_2=0.812$. (a), $k=4$; (b), $k=5$; (c), $k=6$; (d), $k=7$; (e), $k=8$. \circ , BM structure; \square , cucumber; $+$, Ising model; \triangle , 2D hard disk tessellation; — max-entropy principle.

the Bénard-Marangoni structures. Thus the latter can be considered as the canonical example of mosaics. Notably, the occurrence of systematic cell disappearance and division has now been documented in Bénard-Marangoni structures. This study also confirms the fact that peripheral cells introduce an asymmetry of the cell-shape distribution, and an apparent additional disorder.

This study confirms the structural similarity between two-dimensional froths. Most striking is the similarity between the Bénard-Marangoni structures and the cucumber epithelium. This result is remarkable, because the forces involved are completely different. This shows that statistical equilibrium is completely independent of the microscopic interactions which establish it. This observation is at the basis of maximum entropy inference [29,30,34,35].

The concordance between topological characteristics of these natural and model-constructed structures is satisfactory, in spite of the fact that the T_2 process (cell creation or

cell annihilation) is not included in the Ising model [31,32] and in “two-dimensional hard disk tessellations” [24]. Both topological transformations T_1 and T_2 (cell creation and annihilation) are observed in Bénard-Marangoni structures and statistical equilibrium is reached more efficiently [49]. Recently, a model which takes into consideration the two ETT has been proposed by Segel *et al.* [50] to determine the cell-shape and cell-area distributions; they are in good agreement with those of soap froths. Any discrepancies between natural and model-constructed structures regard the cells with $n \neq 6, 5$, or 7 , which are always rare and, in Bénard-Marangoni structures, have a short lifetime.

ACKNOWLEDGMENT

Work in Strasbourg was supported by the EU mobility program, FOAMPHYS Network, Contract No. ERB-CHRXCT 940542.

- [1] D. A. W. Thompson, *On Growth and Form* (Cambridge University Press, Cambridge, 1917).
- [2] D. Weaire, *Metallography* **7**, 157 (1974).
- [3] D. Weaire and N. Rivier, *Contemp. Phys.* **25**, 59 (1984).
- [4] J. L. Meijering, *Philips Res. Rep.* **8**, 270 (1953).
- [5] D. A. Aboav and T. G. Langdon, *Metallography* **2**, 171 (1970).
- [6] I. J. Smalley, *Geol. Mag.* **103**, 110 (1966).
- [7] F. T. Lewis, *Anat. Rec.* **38**, 341 (1928); *ibid.* **50**, 235 (1931).
- [8] J. C. Mombach, M. A. Z. Vasconcellos, and R. M. C. De Almeida, *J. Phys. D* **23**, 600 (1990).
- [9] M. Hasegawa and M. Tanemura, *Ann. Inst. Statist. Math. (Tokyo)* **B 28**, 509 (1976).
- [10] G. Le Caër and R. Delannay, *J. Phys. (France)* **I 3**, 1777 (1993).
- [11] D. A. Aboav, *Metallography* **3**, 383 (1970); **13**, 43 (1980).
- [12] I. K. Crain, *Comput. Geosci.* **4**, 131 (1978).
- [13] B. N. Boots and D. J. Murdoch, *Comput. Geosci.* **9**, 351 (1983).
- [14] G. Le Caër and J. S. Ho, *J. Phys. A* **23**, 3279 (1990).
- [15] F. Rothen and A. J. Koch, *J. Phys.* **50**, 633 (1989).
- [16] J. M. Kosterlitz and D. J. Thouless, *Prog. Low Temp. Phys.* **7B**, 371 (1978).
- [17] D. R. Nelson and B. I. Halperin, *Phys. Rev. B* **19**, 2457 (1979).
- [18] R. Occelli, E. Guazelli, and J. Pantaloni, *J. Phys. Lett.* **44**, L597 (1983).
- [19] N. Rivier, R. Occelli, J. Pantaloni, and A. Lissowski, *J. Phys.* **45**, 49 (1984).
- [20] P. Cerisier, J. Pantaloni, G. Finiels, and R. Amalric, *J. Appl. Opt.* **21**, 2153 (1982).
- [21] P. Cerisier, R. Occelli, C. Pérez-Garcia, and C. Jamond, *J. Phys. (Paris)* **48**, 569 (1987).
- [22] B. Simon and M. Belmedani, *C. R. Acad. Sci. Paris* **319**, 865 (1994).
- [23] F. P. Preparata and M. I. Shamos, *Computational Geometry* (Springer-Verlag, New York, 1985), Chap. 4.
- [24] D. P. Fraser, M. J. Zuckermann, and O. G. Mouritten, *Phys. Rev. A* **42**, 3186 (1990).
- [25] J. Lemaître, A. Gervois, J. P. Troadec, N. Rivier, M. Ammi, L. Oger, and D. Bideau, *Philos. Mag. B* **67**, 347 (1993).
- [26] J. Lemaître, J. P. Troadec, A. Gervois, and D. Bideau, *Europhys. Lett.* **14**, 77 (1991).
- [27] J. C. Earnshaw and D. J. Robinson, *Phys. Rev. Lett.* **72**, 3682 (1994).
- [28] N. Rivier, *Philos. Mag. B* **52**, 795 (1985).
- [29] E. T. Jaynes, *Phys. Rev.* **106**, 620 (1957); **108**, 171 (1957).
- [30] E. T. Jaynes, *The Maximum Entropy Formalism*, edited by R. D. Levine and M. Tribus (MIT Press, Cambridge, MA, 1979); T. J. Lored, in *Maximum Entropy and Bayesian Methods*, edited by P. F. Fougere (Kluwer, Boston, 1990).
- [31] G. Le Caër, *J. Phys. A* **24**, 1307 (1991); **24**, 4655 (1991).
- [32] R. Delannay, G. Le Caër, and M. Khatun, *J. Phys. A* **25**, 6193 (1992).
- [33] B. Billia, H. Jamgotchian, and Thi. H. Nguyen, *Metall. Trans. A* **22**, 3041 (1991).
- [34] M. A. Peshkin, K. J. Strandburg, and N. Rivier, *Phys. Rev. Lett.* **67**, 1803 (1991).
- [35] N. Rivier, *J. Phys.* **4**, 931 (1992); N. Rivier and B. Dubertret, *Philos. Mag. B* **72**, 311 (1995).
- [36] T. Ondarçuhu, J. Millan-Rodriguez, H. Mancini, A. Garcimartin, and C. Pérez-Garcia, *Phys. Rev. E* **48**, 1051 (1993).
- [37] F. T. Lewis, *Am. J. Bot.* **30**, 766 (1943).
- [38] M. B. Pyshnov, *J. Theo. Bio.* **87**, 189 (1980).
- [39] N. Rivier, in *From Statistical Physics to Statistical Inference and Back*, edited by P. Grassberger and J. P. Nadal (Kluwer, Boston, 1994); N. Rivier, G. Schliecker, and B. Dubertret, *Acta Biotheoretica* **43**, 403 (1995).
- [40] G. Le Caër and R. Delannay, *J. Phys. A* **26**, 3931 (1993).
- [41] B. N. Boots, *Metallography* **15**, 53 (1982); **20**, 231 (1982); **18**, 301 (1985).
- [42] N. Rivier and A. Lissowski, *J. Phys.* **15A**, L143 (1982).
- [43] C. Annic, J. P. Troadec, A. Gervois, J. Lemaître, M. Ammi, and L. Oger, *J. Phys. (France)* **I 4**, 115 (1994).
- [44] N. Rivier, *Philos. Mag. B* **47**, L45 (1983).
- [45] J. Von Neumann, in *Metal Interfaces* (Am. Soc. Metal, Cleveland, 1952).
- [46] J. Pantaloni, P. Cerisier, R. Bailleux, and C. Gerbaud, *J. Phys. (Paris) Lett.* **42**, L147 (1981).
- [47] C. Normand, Y. Pomeau, and M. G. Velarde, *Rev. Mod. Phys.* **49**, 581 (1977); P. Bergé and M. Dubois, *Contemp. Phys.* **25**, 535 (1984); F. H. Busse, *Rep. Prog. Phys.* **41**, 1931 (1978).
- [48] E. Bodenschatz, J. de Bruyn, G. Ahlers, and D. S. Cannell, *Bull. Am. Phys. Soc.* **36**, 653 (1991); S. Ciliberto, E. Pampaloni, and C. Pérez-Garcia, *Phys. Rev. Lett.* **61**, 1198 (1991).
- [49] N. Rivier, *Physica D* **23**, 129 (1986).
- [50] D. Segel, D. Mukamel, O. Krichevsky, and J. Stavans, *Phys. Rev. E* **47**, 812 (1993).